Efficient Data Compression for Distributed Detection in Wireless High-Density Arrays: a Simulated Study

J-D. Jutras[1], B. G. Fallone[1,2], and N. De Zanche[1,2]
[1]Dept. of Oncology, University of Alberta, Edmonton, Alberta, Canada, [2]Dept. of Medical Physics, Cross Cancer Institute, Edmonton, Alberta, Canada

Introduction

High-density coil arrays [1,2,3] offer numerous advantages over their standard counterparts including improved signal-to-noise (SNR) ratio and parallel imaging performance. However, with a large number of channels cabling becomes bulky, safety margins are reduced, and coupling between coils and nearby coaxial cables leads to cross-talk that is difficult to manage. Analog wireless and optical fibre links have been considered to eliminate coaxial cables, but limitations in dynamic range and noise figure preclude their use [4,5]. The ideal solution is a fully untethered digital connection between each coil and the spectrometer, which will require digitization and the usual digital demodulation and detection operations to be performed at each coil. This scheme also requires an efficient method of digitally compressing the MR data to allow many channels to be transmitted over the limited data rate of the wireless link (e.g., 54Mb/s for IEEE802.11a, which is readily exceeded in high-bandwidth scans with as few as 10 coils). In this work, we investigate the image artefact power (AP) [6] resulting from two data compression methods: The first takes advantage of the low spectral efficiency present when signal from a coil with a small field-of-view (FOV) is sampled at the full acquisition bandwidth (i.e., as if it were from a volume coil). Since at any instant the signal bandwidth cannot exceed the product $\gamma\cdot|G(t)|\cdot FOV_{coil}$, much of the sampling bandwidth is unused. The second method compresses the dynamic range of the MR signal, reducing the required bit depth. These reductions in data are independent of, and in addition to the reductions obtained from parallel imaging, and can also be used to reduce the memory requirements of large scans.

Methods

Our proof of concept is based on a grid phantom scanned on a Philips Achieva 3T using a 6-channel head array and a spiral readout [7] (maximum gradient strength 21 mT/m, slew rate 100 T/(m s), FOV = 21×21 cm^2, T_R = 500ms, T_E = 1.39ms, T_{acq}= 6.156 ms, BW = 186 kHz, 60 interleaves of 1146 samples). The raw κ-space data, $s(t)$, were processed off-line in MATLAB to simulate the coil-wise operations of dynamic demodulation [8], anti-alias filtering and decimation. The image from coil n is therefore confined to a reduced FOV centered on the weighted centroid of its sensitivity profile, $\mathbf{r}_n$. The demodulated signal is simply $s_d(t) = s(t)\exp(-i\boldsymbol{\kappa}(t)\cdot\mathbf{r}_n)$, which may be interpreted as the Fourier shift theorem generalized to an arbitrary κ-space trajectory $\boldsymbol{\kappa}(t)$. This signal is then anti-alias filtered and down-sampled by a factor M<1 (MATLAB function *resample*), resulting in a spectrally compressed version of the original signal. Bit depth reduction was performed by applying sampling density compensation [9] to the spiral signal (compressing dynamic range by 27.5 dB) and zeroing the k least-significant bits (originally 16 bits/quadrature component/sample). Reconstruction requires up-sampling and re-modulating back to the original FOV followed by standard gridding onto a 256×256 matrix (e.g., non-uniform FFT [10]) and array image combination (root-sum-of-squares).

Results and Discussion

Aliasing due to spectral compression becomes visible at a threshold AP=3.5×10^{-4} (dashed line in Fig. 1a). Consequently, the maximum down-sampling factor that can be tolerated after dynamic demodulation was chosen as M=55% (AP=3.15×10^{-4}). Ghosting due to bit depth reduction becomes visible at a threshold AP=2×10^{-4} (dashed line in Fig. 1b), and the maximum number of bits that can be zeroed was found to be $k = 6$ (AP=1.69×10^{-4}). The image in Fig. 2a is reconstructed from the full dataset for comparison with the image reconstructed following both types of data compression (Fig. 2b). Despite the fact that only 34% of the original amount of data memory is needed, image quality is fully preserved (AP=3.51×10^{-4}), with no degradation in contrast or SNR. Without dynamic demodulation prior to anti-alias filtering and down-sampling, visible aliasing (AP=1.8×10^{-3}) results in the reconstructed image (Fig. 2c). Likewise, no dynamic range compression before bit depth reduction results in visible ghosting (AP=8×10^{-3}) (Fig. 2d).

Conclusion

We have shown that the amount of data transmitted wirelessly from a coil array to the image reconstruction console can be reduced significantly using spectral and dynamic range compressions while maintaining equivalent image quality. Much greater compression performance is expected from high-density arrays due to the smaller size of the coil FOV relative to that of the acquisition FOV. These methods are not limited to spiral trajectories and can be applied to others such as Cartesian (spectral compression reduces to the PILS technique [11]) along with appropriate dynamic range compression (e.g., dynamic gain adjustment [12]). These compression techniques can be implemented on fast digital processing hardware such as FPGAs or ASICs.

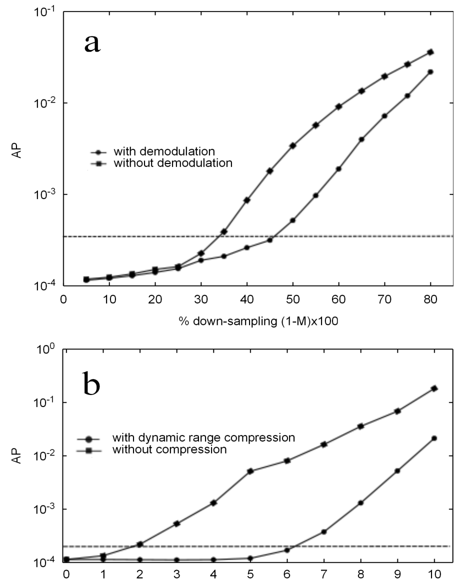

Figure 1: Artifact power (AP) as a function of: **a)** percent down-sampling for spectral compression and **b)** number of zeroed bits for dynamic range compression. Dashed lines are maximum tolerable AP.

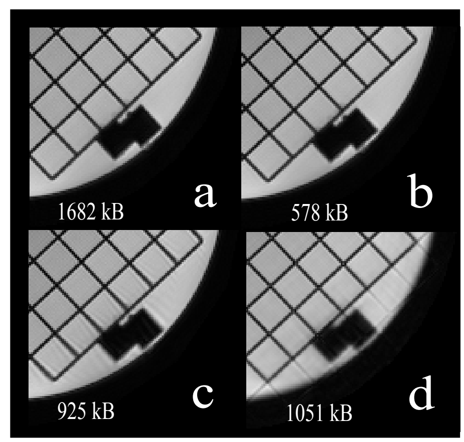

Figure 2: Detail of the grid phantom, showing: **a)** image reconstructed from the full dataset without compression, **b)** image reconstructed following both dynamic range and spectral compression, **c)** image reconstructed following spectral compression but without prior dynamic demodulation, resulting in aliasing artifacts, **d)** image reconstructed following bit-depth reduction, but without prior dynamic range compression, resulting in ghosting artifacts.

References

1. Magn. Reson. Med. 59(6) pp.1431-1439. **2.** J. Magn. Reson. Imag. 28(5) pp.1219-1225. **3.** Magn. Reson. Med. 62(3) pp.754-762. **4.** J. Magn. Reson. 186(2) pp.358-363. **5.** J. Magn. Reson. 189(1) pp.130-138. **6.** Magn. Reson. Med. 53(1) pp.186-193. **7.** MAGMA 9(1-2) pp.29-41. **8.** Magn. Reson. Med. 54(3) pp.669–676. **9.** IEEE Trans. Med. Imag. 18(5) pp. 385-392. **10.** SIAM J. Sci. Comput. 21(1) pp. 283-293. **11**. Magn. Reson. Med. 44(4) pp.602–609. **12.** Concepts Magn. Reson. Part A. 36A(4) pp.243-254.

Acknowledgements

We acknowledge funding from the Alberta Cancer Research Institute and Natural Sciences and Engineering Research Council (Canada). We thank Philips Healthcare for technical support and Dr. Roger Luechinger for the PATI program used for data transfer. This work was initiated by stimulating discussions with Dr. Klass Pruessmann.